工学部SSSVプログラム
日中共同セミナー

（２０１２年9月１９日―9月２７日）

Researches on the micro-structured fiber gratings and their applications to high sensitive fiber sensors and all-optical signal processing devices

Hongpu Li

Faculty of Engineering, Shizuoka University, 3-5-1, Johoku, Hamamatsu, 432-8561, Japan

ABSTRACT

- Calibration of a phase-shift formed in a linearly chirped fiber Bragg grating by using wavelength-interrogated fiber ring laser and its application to temperature sensor
- Cladding mode coupling in a wide-band fiber Bragg grating and its application to a power-interrogated temperature sensor
- Phase shifted and cascaded long-period fiber grating written by using focused high-repetition-rate CO2 laser pulses
- Long period fiber grating and its application to all-optical pulse shaping
- Fabrication of micro/nano fiber by using focused high-repetition-rate CO2 laser pulses

Investigation of the phase-shift formed in a linearly chirped fiber Bragg grating by using power-interrogated fiber ring laser

Lunlun Xian[1] and Hongpu Li[2]
[1]Graduate School of Science and Technology, [2]Department of Electrical and Electronic Engineering, Faculty of Engineering, Shizuoka University, Johoku 3-5-1, Hamamatsu, 432-8561, Japan

1. Introduction

Phase-shifted fiber Bragg grating (FBG) has been comprehensively studied and widely used in the fields such as the fiber lasers, DWDM filter, etc. [1, 2]. However until present, quantitative analyses on the calibration of the resulted phase-shift and a relationship between the transmission (strength) of the resulted notch filter and the amount of the phase-shift have rarely been given at all. In this paper, relationship between the phase-shift and the strength of the resulted narrow filter is theoretical and experimental demonstrated. Furthermore, a novel scheme which is based on the utilization of a power–interrogated fiber ring laser working for the calibration of the induced phase-shift is experimentally demonstrated.

2. Experimental setup and results

It is found that there existed a beautiful one-by-one relation between amount of the inserted phase-shift and the transmission of the resulted band-pass filter in theoretical analysis, although it is nonlinear one. Here we perform the experimental tests for a linearly chirped FBG (provided by TeraXion Inc.) with different amounts of the phase shift introduced by a PZT, which is shown in Fig.1 Characteristics for this utilized grating have been described in details in [2]. The transmission magnitude increases in accordance with the PZT voltages, it reaches the maximum when the applied voltage is about 160V corresponding to the case where π phase shift is originated.

The one-by-one relationship between the transmission of the narrow band-pass filter and the phase-shift induced in the FBG means that one can indirectly know the amount of the phase shift in a FBG induced by PZT once the transmission of the band-pass filter is precisely measured. To verify the proposal, an Erbium-doped-fiber (EDF)-based fiber ring laser capable of working at single-longitude-mode (SLM) is utilized here. Figure 2 shows the schematic diagram of the experimental setup. In this experiment, the 980nm-LD pump power is kept as a constant of 100 mW. In order to show well the dependent of the laser output on the PZT voltage, we summarized all the data and redraw them in Fig. 3. After the interpolate operation to the data shown in Figs. 1-3, It is easy to find the one-by-one relationship between the laser output power and the induced phase-shift in the FBG, which is shown in Fig. 4.

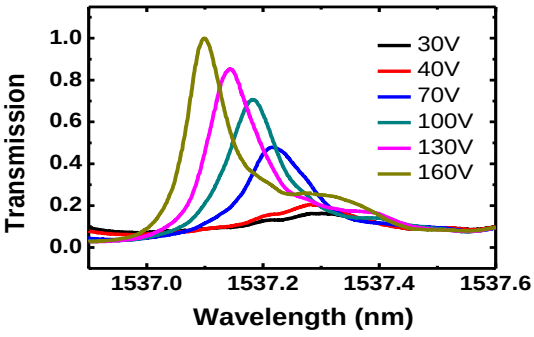

Fig.1. Measurement results for the spectra of the narrow band-pass filter while different PZT voltages are applied.

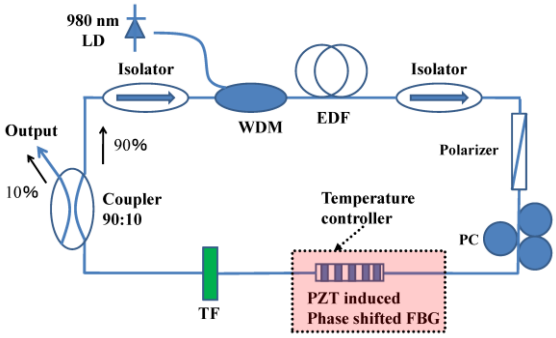

Fig.2. Experimental setup for the SLM EDF ring laser.

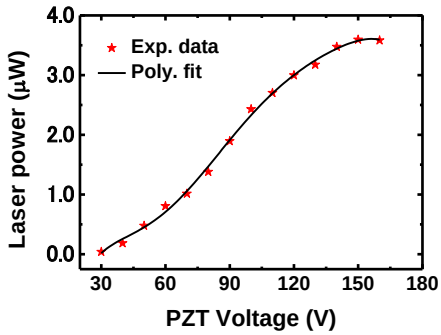

Fig.3. Dependent of the laser output power on the amount of the voltage applied on PZT.

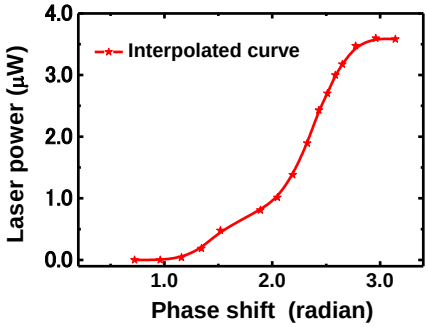

Fig.4. Dependent of the laser power on the amount of the phase shift induced in the FBG.

3. Conclusion

The relationship between the amount of the induced phase-shift in a linearly chirped FBG and reflection of the resulted narrow bandpass filter is theoretical and experimental demonstrated. A novel scheme based on the utilization of a power–interrogated fiber ring laser for quantitative calibration of a phase-shift is numerically and experimentally demonstrated.

References

1. M. Guy, et al., Electron. Lett., vol. **31**, 1924-1925 (1995).
2. X. Chen, et al., J. Lightw. Technol., **28**, 2017–2022 (2010).

Fabrication and characterization of micro-ring optical resonator based on As_2Se_3 glass

Masahiro Fukuyo[1] and Kazuhiko Ogusu[2]
[1]Graduate School of Science and Technology, [2]Department of Electrical and Electronic Engineering, Faculty of Engineering, Shizuoka University, Johoku 3-5-1, Hamamatsu, 432-8561, Japan

1. Introduction

Optical fiber technology is used, such as Silicon as how to send information to the recent large capacity has been widely used, it has become essential to modern technology. On the other hand, in that require improvement in signal processing speed due to the large capacity of information, the signal processing by the electrical signal is limits at 10Gbit / s, the signal processing by light, the transmission rate of more of the all optical device that is take advantage has been attracting attention. All-optical devices are required to be low-loss communication wavelength band and high nonlinearity. In this research, we fabricated micro-ring resonator using As_2Se_3 glass, check the bistable operation.

2. Fabrication for As_2Se_3 waveguides

The waveguide structure is fabricated waveguide layer based the Ag-As_2Se_3, as shown in Fig.1. This waveguide was tuned wavelength in 1.064μm. This waveguide is composed of the substrate is silicon wafer, the lower cladding layer is PMMA, the waveguide layer is Ag-As_2Se_3 and the strip layer is As_2Se_3. Then, thickness of the waveguide layer d is 0.40μm, thickness of the strip h is 0.05μm and waveguide width w is 2.0μm.The fabrication process of the waveguide has eight steps. The first step is Silicon Wafer coated with PMMA. The second and third step is deposited As_2Se_3 and Ag. The fourth step is Ag-As_2Se_3 was fabrication by photo-doping. The fifth step is it coated with OFPR. The sixth step is the pattern exposed to the sample. The seventh step is deposit As_2Se_3 again. The last step is Lift off OFPR. Fig.2 is micro-ring resonator structure. We depicted the eighteen types of waveguide to a sample. Coupling unit interval D is 1.0, 1.5, and 2.0μm. Length of the coupling Lc is 4, 5, 6, 7, 8, and 9μm. Radius of ring R is 100μm.

3. Experimental setup and results

The experimental setup for measurement of the ring resonator is shown in Fig.3, where the input light is generated by tunable laser, which is varied 1063 to 1065. It gets through beam splitter and half-wave plate, and focused by 60 times lens. Fig4 is spectral response of ring resonator. Resonance wavelength interval was 0.38nm, 0.34nm and 0.37nm.The resonant depth was about 3dBm to 1dBm.

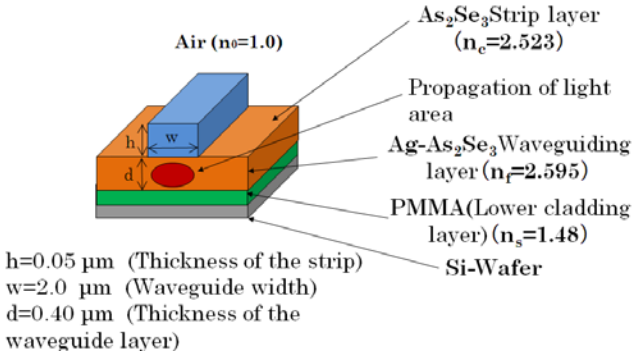

Fig.1. Waveguide structure.

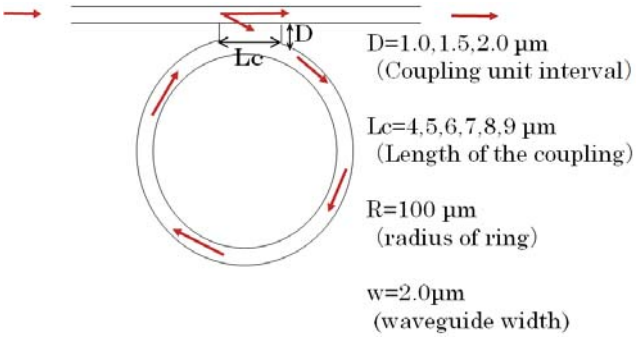

Fig.2. Micro-ring resonator structure.

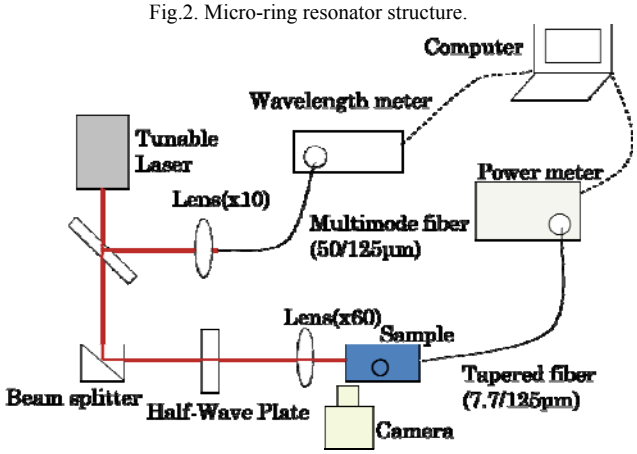

Fig.3. Experimental system for the measurement of the resonance characteristics.

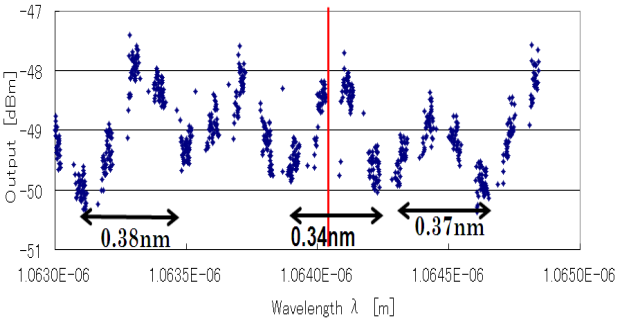

Fig.4. Measurement results for spectral response of ring resonator.

4. Conclusion

We were able to establish the fabrication technology of the ring resonator to measure the transmitted power. Resonate characteristics, depth of the resonance of up to 3dBm. Cause of many variations of the measurement was considered to be not only the fundamental mode propagating and other modes.

Fabrication of a long-period fiber grating by using CO_2 laser

Keisuke Hishiki
Department of Electronic Engineering, Shizuoka University

1. Introduction

Recently, device which used optical fiber are studied for taking much notice of many applications. For example, long-period fiber gratings (LPG), fiber Bragg grating (FBG), nano fiber, and so on. The phase-shifted long fiber (PSLPG) is inserted the shift in LPG. Above all, LPG and PSLPG have many applications, such as band reject filters, gain spectrum flattening filter and temperature sensor, pulse shaping device respectively. So, LPG has been already studied and has been succeed to fabricate by expose photosensitive fiber to ultraviolet. However, it is not yet about general fiber. In this study, LPG is fabricated by irradiate general fiber with CO_2 laser.

2. Experimental setup

The experimental setup is shown in figure 1.The CO_2 laser beam through the shutter is reflected by the mirror on the stage and focus the beam on the fiber by a spherical lens. The fiber is clamped the fiber alignment stage. To measure the transmission spectrum of the LPG, the fiber is connected between an amplified spontaneous emission (ASE) and an optical spectrum analyzer (OSA). Exposing the fiber to the CO_2 laser, refractive index of the fiber core change (increase) for producing the stress In order to realize a periodic refractive index structure, the shutter is possible on/off and the stage is available to move, they are controlled by Lab-view (PC soft). The CO_2 laser works at a typical frequency of 5kHz and duty-cycle is changeable between 0% and 95%. The beam is focused though the spherical lens with a focus length of 70 cm, the minimum spot size on the fiber is about 100 μm .

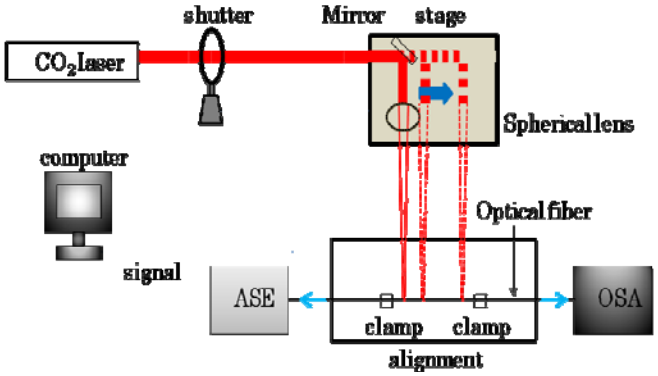

Fig.1 experimental setup

3. Principle

LPG has a periodic effective refractive index change of the fiber core. Its characteristics have the loss peak in specific wavelength when we input the light having normalized intensity. And PS-LPGs have also this characteristic, but it differs from LPGs in terms of being divided the wavelength. These spectral are changed by the distance which I insert. Two cases are considered by the distance inserted. PSLPG is when the inserted distance is shorter than grating period(Λ), and cascaded long period fiber grating (CLPG) is when the inserted distance is much larger than Λ. These LPGs is generated mode coupling to as two grating connected in series. In the principle of these LPGs, core mode is coupled with cladding mode for the first grating edge, it propagates directly in no grating area, the generated cladding mode is coupled with core mode again. So, this works to look like Mach-Zehnder interferometer.

The wavelength of LPGs is satisfied with $\lambda=(n_{core}-n_{clad})\Lambda$ when solve phase matching condition, where n_{core} and n_{clad} is effective refractive index of the fiber core and that of clad, respectively. In this study, I think three typical types, LPG, PSLPG, and CLPG as follow. I use the single mode fiber have n_{core}=1.455 and n_{clad} = 1.453. So, whenλequal to 1550nm , Λ= 630μm. Therefore, we apply to this value for simulation and experiment in all LPGs. In CLPGs, peak wavelength difference are satisfied with $\Delta\lambda=\lambda^2/(n_{core}-n_{clad})\,d$. The smaller Δλ is, the better sensitivity.

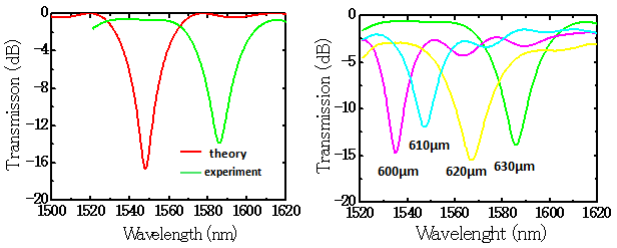

Fig.1 Measured spectral of LPGs

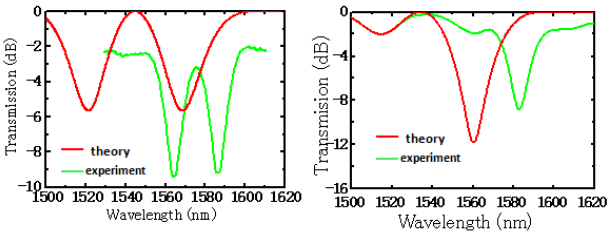

Fig.2 Measured spectral of PSLPGs for π shift and π /2 shift

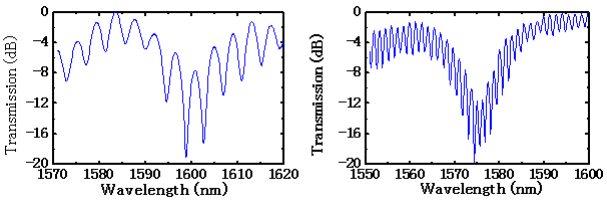

Fig.3 Measured spectral of CLPGs for d=10.6cm and 37.1cm

4. Conclusions

Three kinds of LPGs have been successfully fabricated by using the CO_2 laser from Fig.1 to Fig.3. It is found that characteristics of PSLPG and CLPG spectral strongly depend on the magnitude of the inserted phase shift in a LPG. You can see that the wavelength of LPGs rely on the grating period from Fig.1 left. Resonant wavelength of all LPGs slightly increases the period because of applying the strain to the fiber. In Fig.3 characteristics change by the distance (d).

Reference

[1] Y. J. Rao, et al., Opt. Communications, **229**, 209 (2004).
[2] R. Slavik, et al., Opt. Express, **14** , 10699 (2006).
[3] H. Ke et al., IEEE Photon. Techn. Lett. **19**, 1596 (1998).

Optical bistability in a Fabry-Perot resonator using a nonlinear fiber

Yuki Iwamuro and Kazuhiko Ogusu

Graduate School of Science and Technology, [2]Department of Electrical and Electronic Engineering, Faculty of Engineering,

Shizuoka University, Johoku 3-5-1, Hamamatsu, 432-8561, Japan

1. Introduction

When a high density power enters the medium which has high nonlinearity, the individual input-output characteristic can be obtained. This characteristic is called the optical bistability. It has two stable states by one input. And it can be obtained the limiting characteristic or differential amplify characteristic if change the conditions. We can apply these characteristics to optical switch, linear amplifier, or optical power limiter. These devices are called all optical devices, which can realize the very fast operating device.

In this paper, we investigate the optical bistability using a As_2S_3 fiber Fabry-Perot resonator numerically and experimental setup.

2. Modeling for the Fabry-Perot resonator

Fabry-Perot resonator is constructed by a medium and two mirrors. This resonator can be constructed only put the medium between mirrors. This resonator needs the mirror which has high reflectivity. In this study, we make the mirrors dielectric multilayer [1] on the edge of the fiber by vacuum evaporation. In order to get a reflectivity over 90% and the wavelength which is peak of the reflectivity is around 1060nm, we use the materials of the multilayer are ZnS (refractive index is 2.32) and MgF_2 (refractive index is 1.38). The thickness of the each layer are 91.7nm (ZnS) and 154.2nm (MgF_2) respectively, the number of layer is 7.

In the Fabry-Perot resonator, the output field $E_{out}(t)$ is given by

$$E_{out}(t) = TE_{in}(t - t_R)\exp[-j\{\varphi_0 + \varphi_{NF}(t - t_R)\}] + RE_{out}(t - 2t_R)\exp[-j\{2\varphi_0 + \varphi_{NF}(t - t_R) + \varphi_{NB}(t - 2t_R)\}] \quad (1)$$

where $t_R = nL/c$ is the cavity transit time, R (=r2) is the reflectivity of the mirror, T (=1-R) is transmissivity of the mirror, $\varphi_0 = nk_0L$ is the linear phase shift, $\varphi_{NF}(t - t_R)$ and $\varphi_{NB}(t - 2t_R)$ are the nonlinear phase shifts of the forward and backward propagating wave in the medium, respectively, given by

$$\varphi_{NF}(t - t_R) \approx \frac{n_2 k_0 L}{2\eta_0 T}\{(1 + R)|E_{out}(t)|^2 + R|E_{out}(t - 2t_R)|^2\} \quad (2)$$

$$\varphi_{NB}(t - 2t_R) \approx \frac{n_2 k_0 L}{2\eta_0 T}\{|E_{out}(t)|^2 + (1 + R)|E_{out}(t - 2t_R)|^2\} \quad (3)$$

where k_0 is the wave number, η_0 is the wave impedance in the vacuum, n_2 is the nonlinear refractive index of the medium [2]. The result of the calculation for optical bistability is shown in Fig. 1. In Fig.1 (a), the optical bistability is obtained when the cavity length is 1mm, reflectivity of the mirror is 90%, initial detuning is -0.1π, input pulse width is 0.5ns, and input power is 1mW. Fig.1 (b) shows the dependent of the characteristic on change of the initial detuning. When the initial detuning is -0.2π, we can obtain the good bistability, and the initial detuning is -0.4π, the characteristic is linear.

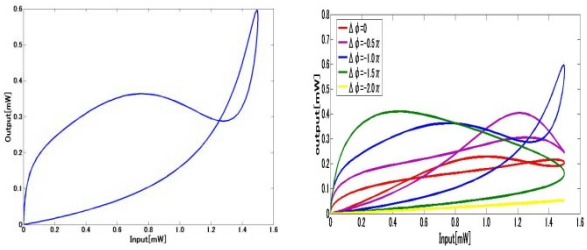

(a) (b)

Fig.1 Input-output characteristic

3. Experimental setup

Fig. 2 is the experimental setup for observing optical bistability. The light source is the laser which generates the pulse its width is 500ps and repetition rate is 10Hz at the 1.064 μm. In order to get the detuning, one mirror is made on the edge of the SiO2 single mode fiber at the side of the input and the other mirror is made on the edge of the As2S3 fiber which can be moved by the actuator at the side of the output.

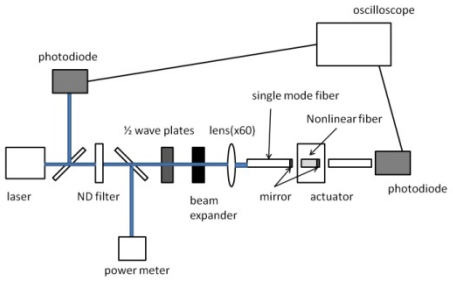

Fig.2 Experimental setup for observing optical bistability

4. Conclusions

Optical bistability in the As2S3 fiber Fabty-Perot resonator has been numerically investigated. In order to realize the optical bistability, we must make the mirror with more high reflectivity mirror. So we must adjust the layer thickness of multilayer and make the mirror more clearly.

References

[1] S. J. Orfanidis "Electromagneti c waves and Antennas",(2008)

[2] K.Ogusu, et al Jpn. J. Appl. Phys. Vol. 42 pp. 434-438 (2003)

Cladding mode coupling in a wide-band fiber Bragg grating and its application to a power-interrogated temperature sensor

Peng Wang and Hongpu Li

1. Introduction

Investigations for the cladding mode influence on the spectrum of a linearly chirped FBG with bandwidth larger than 10 nm, based on the cladding-mode coupling phenomenon, a novel FBG-based all-fiber sensor enabling to measure temperature within the range of 17-180 ^{o}C is firstly proposed and successfully demonstrated by using power-interrogation technique instead of the spectrum-shift measurement with a optical spectrum analyzer (OSA)

2. Principle and experimental setup

We perform various investigations to the temperature performance of the setup shown in Fig. 1, where the FBG is located in a temperature chamber and the temperature can bediscretely changed between 17^{0}C to 180^{0}C.

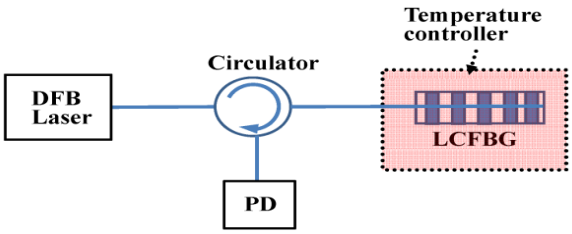

Fig. 1. Experimental setup for the temperature measurement based on the power-interrogated method.

The results are shown in Fig. 2. It can be seen that the as the temperature is increased, the spectra is right shift with a thermal responsibility about 10.85 pm/^{0}C, which is nearly the same quantity as those reported before. To guarantee the setup (shown in Fig. 1) works in a linear region corresponding to the wavelength in the range of 1537.5 nm to 1540.6 nm as is shown in Fig. 2, the working wavelength of the DFB laser is fixed and set in advance as 1540.60 nm. Figure 3 shows the measuring results for the change of the output power (PD) vs. temperature change. It can be seen that as expected, almost a fine linear relationship between the laser power at the port of PD and the ambient temperature of the grating has been obtained and the thermal responsibility is about 0.01626dB/^{0}C Moreover, unlike most the FBG-based sensors reported before [1-2], here the utilized FBG is functioned simultaneously as both the sensing and the interrogating element.

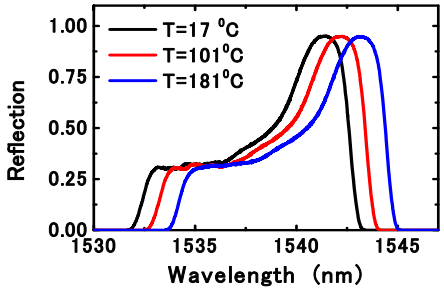

Fig. 2. The reflection spectra of the utilized LCFBG at three different temperatures, 17, 101, and 180 ^{0}C, respectively

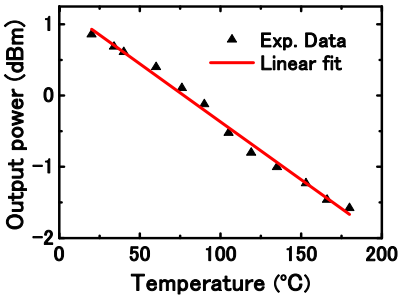

Fig. 3. Measurement results for the dependence of the output power vs. the temperature

3. Conclusion

Based on this phenomenon, a novel FBG-based sensor enabling to measure temperature in the range of 17-181^{0}C is firstly demonstrated just by using a power-interrogation technique. Unlike most of the previous FBG-based sensors, here the utilized FBG is functioned as both the sensing and interrogating element, which considerably simplifies the sensing system and make it more compact and the least cost.

References

[1] W. W. Morey, et al. *SPIE Fiber Optic & Laser Sensors VII,* 1169，(1989)

[2] S. M. Melle , et al. *IEEE Photon. Technol. Lett.*, 516–518(1992).

Fabrication of Cylindrical Opals and Inverse Opals and Their Optical Properties

Chen Wei Wang Ming

(*Key Laboratory on Opto-Electronic Technology of Jiangsu Province, School of Physics Science and Technology, Nanjing Normal University, Nanjing 210046, China*)

1. Introduction

Microstructure optical fibers (MOFs) have exhibited many novel optical properties in recent years. Photonic band gap fibers (PBGFs) with hollow core guiding structures are a kind of microstructure optical fibers (MOFs) to overcome the limitations of traditional silica optical fibers. Many efforts have been made to fabricate 3DPBGFs: E. Valdivia et al. coated a standard optical fiber with three dimensional colloidal crystals which could be used as a template to form inverse opal hollow core PBGFs[1]; S.-M. Yang et al. created polymer hollow cylindrical structures with three dimensionally interconnected air cavities by infiltrating polymer precursor into a colloidal crystal template on fibers which was fabricated by dip-coating method[2].

2. Experimental setup and results

Capillaries were cleaned in an ultrasonic bath fist using acetone and then deionized (DI) water for 10 minutes respectively. Then cleaned capillaries were dried with nitrogen before use. To fabricate opals on the internal surface of capillaries, PS colloidal solution dispersed in DI water with concentration of ~1vol % was injected into a capillary. The height of the solution inside the capillary is 10-95mm and can be precisely controlled by a micro-pump. One end of the capillary was sealed to control the evaporation direction of solvent. Fig1 (a) shows a schematic diagram of fabrication opals on a capillary internal wall and Fig1 (b) is a schematic diagram of colloidal crystal growth on a capillary internal wall with vertical deposition method. Fig1 (c) is cross section view the capillary internal wall coated with opals. Fig2 is schematic diagram of transmission spectrum measurement. Transmission spectrum was measured with a YOKOGAWA optical spectral analyzer (AQ6370). The YOKOGAWA white light source (AQ4305) was coupled into a multimode optical fiber and focused to inverse opals at normal incidence with a couple of collimating lens. Transmitted lights were focused to the optical spectral analyzer by a lens.

Fig3 (a)~(d) are images of opals on the internal wall of a capillary assembled from 490nm PS microspheres. (a) and (b) are optical microscope images observed in reflection mode, (c) are SEM images of opals on the internal wall of a capillary, inset is high magnification of internal wall，(d) top cross section surface of the opals inside a capillary and inset is high magnification of the cross section.(e)~(h) are images of 490nm silica inverse opals on the internal wall of a capillary with sol-gel co-assembly method. (e) are bare capillary and internal wall coated with composite colloidal crystal, (f) internal wall preserved with silica inverse opals after sintering and bare capillary. The axial uniformity together with the symmetric color distribution on the capillary internal edges attests to the high quality of composite colloidal crystal, which spectrally shifts the stop band with the viewing angle around the capillary curved surface. The color on the internal edge of the capillary has a blue shift after removing the PS colloidal crystal template as the effective refraction index decreased. (g) longitudinal section of the capillary whose internal wall coated with silica inverse opals, inset is high magnification of internal wall. In the inset uniform small pores on the bottom of the big pores can be seen obviously which show the good connectivity of the air spheres.(h) cross section of inverse opals and the high magnification of the cross section.

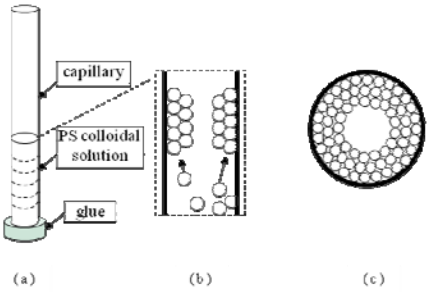

Fig1.Fabrication schematic diagram

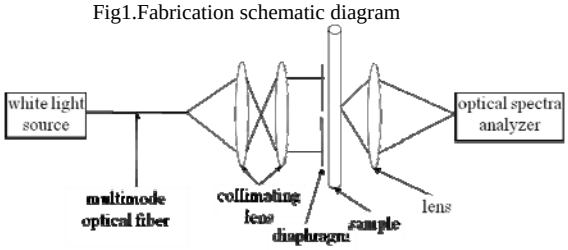

Fig2 Schematic diagram of transmission spectrum measurement

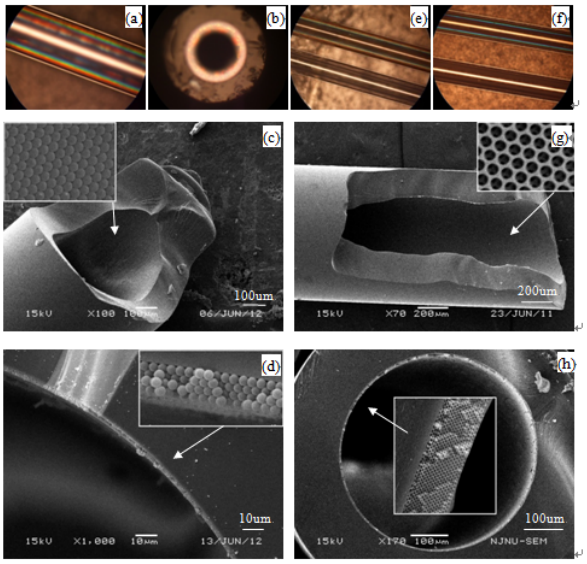

Fig3. Images of opals on the internal wall of a capillary assembled from 490nm PS microspheres

3. Conclusion

Hollow cylindrical opals and inverse opals have been made by self-assembly method in a capillary. With vertical self-assembly method hollow cylindrical PS opals and SiO2 inverse opals films of different radiuses have been made in capillaries with same radiuses. According to microstructures and optical performance of fabricated samples, radius of curvature basal and diameter of microspheres used are main factors affect the film structure and optical performance. The complete solution states change have been discussed. Scanning electron microscope is used to character its internal structures.

References

[1] J. Li, et al., Opt. Express **13**, 6454-6459 (2005),

[2] J. H .Moon et al., Journal of Colloid and Interface Science **287**, 173-177 (2005).

The design and simulation of the accelerometer

You Jingjing and Wang Ming
Key Laboratory on Opto-Electronic Technology of Jiangsu Province, School of Physics Science and Technology,
Nanjing Normal University, Nanjing 210046, China

1. Introduction

The miniature fiber optic sensor based on Fabry-Perot (F-P) interferometry reported is designed for vibration monitoring applications. The sensor used for this application is not only safety and cost economics , but also unaffected to radiation or high electromagnetic fields .

2. The structure design of the accelerometer

The designed structure of the accelerometer is composed of SU8 diaphragm with four beams clamped around and the commercial fiber. The schematic diagram of the accelerometer and the SU8 diaphragm with four beam around clamped are shown in Fig.1 .The F-P cavity is composed of the terminal face of the fiber and the subdiaphragmatic surface . SU8 diaphragm has very excellent imaging characteristics , and it is capable of producing very high aspect ratio structures . Commercial fiber is used to transfer incident and reflected light .

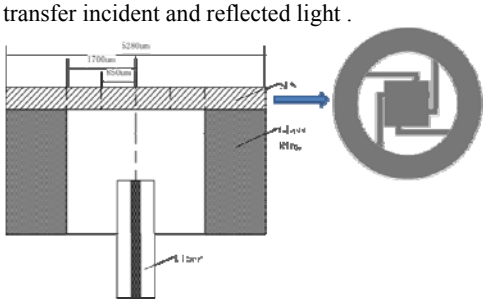

Fig.1. The schematic diagram of the accelerometer and the SU8 diaphragm with four beam around clamped .

3. The theory of the accelerometer

In the spring mass system with one degree of freedom loaded a simple harmonic excitation in the substrate[1], the relative displacement of the mass is as followed:

$$X = \frac{A\omega^2}{\omega^2\sqrt{(1-\gamma^2)^2+(2\xi\gamma)^2}} = \frac{\ddot{y}_{max}}{\omega^2\sqrt{(1-\gamma^2)^2+(2\xi\gamma)^2}} \tag{1}$$

and ,

$\xi = \frac{c}{2m\omega}$,is the damping ratio ;

$\gamma = \frac{\theta}{\omega}$,is frequency ratio，which is the ratio of the external excitation frequency dividing by the natural frequency of the system;

$\omega^2 = \frac{k}{m}$,w is the natural frequency.

As γ nearly equal to zero , we can get equation(2) ,

$$X \approx \frac{\ddot{y}_{max}}{\omega^2} \tag{2}$$

The value of X is in direct proportion to the acceleration amplitude .It is the principle of the accelerometer .

4. The simulation of system characterization

A model of the designed structure is established and simulated by CoventorWare , which is shown in Fig.2 . In the simulation ,a simple harmonic excitation loads in the bottom face of the modal , that can cause the SU8 diaphragm vibrating according to the theory of the accelerometer.

From the simulation, we captured a diagram of the maximum displacement in the z direction caused by the harmonic excitation, shown in the Fig.3 .The blue curve stands for the displacement of the fiber terminal surface , and the red curve stands for the displacement of the subface of the SU8 diaphragm . Therefore , the difference between the two curves is the length of the F-P cavity . We can get the changing length of the F-P cavity 30.7369μm , and the response ratio about 100nm/10hz in the range of 0 to 3000 hz .

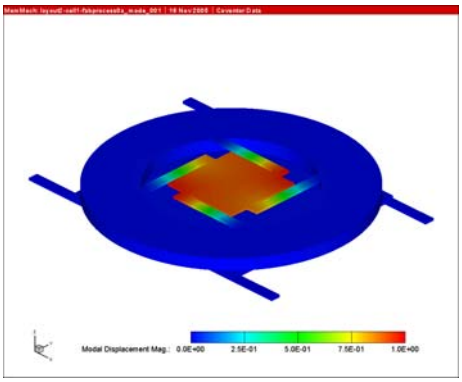

Fig.2. The modal of the designed structure with a harmonic excitation loading in the subface of the structure .

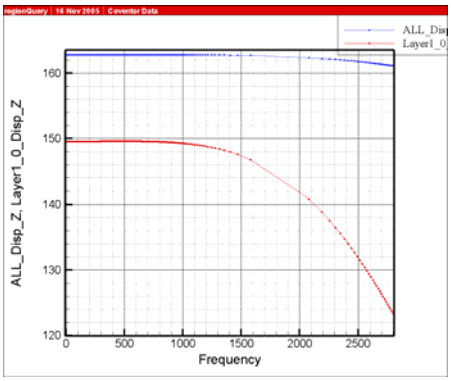

Fig.3. The maximum displacement of two points in the z direction caused by the harmonic excitation .

5. Conclusion

With the help of polymer MEMS technology, the high aspect ratio structure is feasible and realizable. Through our work, the design structure can meet the condition of vibration measuring . However , the vibration measuring is a complicated process, and the parameter of system is remained to be further determined.

References

[1] Jesus M. Corres ,Sensors and Actuators A 132 (2006) 506–515

Measurement of Fiber Length Using Passively Mode Locked Fiber Laser with a Semiconductor Saturable Absorber Mirror

Congcong Zhang[1], Ming Wang[2*]

[1] School of Physical Science and Technology, Jiangsu Key Lab on Opto-Electronic Technology, Nanjing Normal University, Nanjing 210046, P. R. China, 15950562770, 025-83598685

[2]School of Physical Science and Technology, Jiangsu Key Lab on Opto-Electronic Technology, Nanjing Normal University, Nanjing 210046, P. R. China, 025-83598685,025-83598685

1. Introduction

This paper investigates the passively mode-locked erbium-doped ring fiber laser with a semiconductor saturable absorber mirror and its application for measurement in Fiber Length. Using a semiconductor saturable absorber mirror (SESAM), a passively mode-locked fiber ring laser was demonstrated and stable sub-picoseconds pulses were produced. A new method for measuring optical fiber length using an all-fiber mode-locked laser with the semiconductor saturable absorber mirror was presented.

2. Experimental setup and results

Using a semiconductor saturable absorber mirror (SESAM), a passively mode-locked fiber ring laser was demonstrated and stable sub-picoseconds pulses were produced. This ring fiber laser was constructed with a WDM（Wavelength Division Multiplexing）, erbium-doped fiber as gain medium as well as circular, polarization controller, and coupler. In experiments, the fiber laser operated stably with mode-locked pulse laser output whose peak wavelength of 1558nm, spectrum width of 7.2 nm without any satellite pulses or pedestal, repetition frequency of 7.75 MHz and maximum mean optical power of 2.6 mW. It was found that the characteristics of the output laser pulse in time domain would change a little while adjusting the polarization controller in experiments. The pulses was measured by an oscilloscope and a frequency spectrograph, and theoretically the pulses were as narrow as 347 fs. During long time, the laser can work stable. The experimental setup was simple, compact, and self-started. The experimental results are helpful to the use of semiconductor saturable absorber mirror in passively mode-locked fiber laser.

Optical fiber is the best media in modern communication networks for its characteristics of low loss and wide frequency band. Precise measurement of optical fiber length is a fundamental technique in many areas, such as in optical communications and fiber-optic sensing networks. A new method for measuring optical fiber length using an all-fiber mode-locked laser with the semiconductor saturable absorber mirror was presented. The semiconductor saturable absorber mirror can act as the saturable absorber for mode-locking with nonlinear polarization rotation based on the random birefringence of the single-mode fiber. The mode-locked fiber laser has the all-fiber nature and can be stable for a long term. Since the transit time in cavity corresponding to the fundamental frequency is exactly linearly proportional to the cavity length of the mode-locked fiber laser, a novel simple method to measure the fiber length has been experimentally demonstrated using a mode-locked fiber laser configuration. Compared to presented methods, there is no dead zone in our method and no limitation in measuring fiber length over hundreds of kilometers due to low insertion loss and direct splicing into an all-fiber system. First we test single fiber with several lengths from about 100 orders of magnitude to about several meters. Then we test the system with many ways. The result shows our system has a large measurement range and high precision. The experimental setup was simple and easy to test. We call this as the mode-locking method. It has a high value in practical and can be used in the actual construction as we can see.

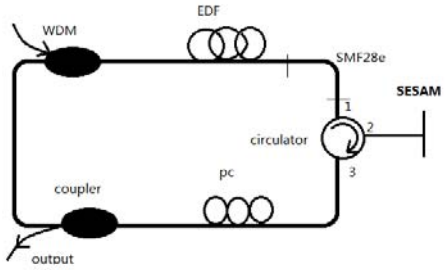

Fig.1.Experimental for the passively mode locked fiber laser

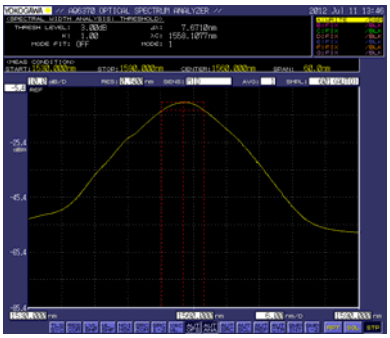

Fig.2. The spectrogram of passively mode locked fiber laser

3. Conclusion

A passively mode-locked erbium-doped ring fiber laser with a semiconductor saturable absorber mirror is demonstrated in experiment. A new method for measuring optical fiber length using an all-fiber mode-locked laser with the semiconductor saturable absorber mirror was presented. It has a high value in practical and can be used in the actual construction.

References

1. U Keller;D A B Miller;G D Boyd, Solid-state lowloss intracavity saturable absorber for Nd:YLF lasers:an antivesonant semiconductor Fabry-Perot saturable absorber, *Optics Letters*, 1992, **Vol. 17(7),** pp. 505-507,
2. De Souza, E.A.: Soccolich, C.E., Saturable absorber modelocked polarisation maintaining erbium-doped fibre laser, *Electronics Letters*, 1993, **Vol. 29(5),** pp. 447-449.
3. WANG Jing, ZHANG Hong-ming, ZHANG Jun, YAN Meng, YAO Min-yu, Passively Mode-Locked Fiber Laser with a Semiconductor Saturable Absorber Mirro, *Chinese Journal of Lasers*, 2007(02),
4. ZHANG Zh X;WU J;XU K, Multiple output states from passive mode-locked fiber lasers, *laser technology*, 2009(05),

Self-mixing interferometer based on sinusoidal phase modulating technique

Zhenyu Yang[1], Ming Wang [2], Wei Xia[1]
[1] Graduate School of Physical Science and Technology,[2] Jiangsu Key Lab on Opto-Electronic Technology,
Nanjing Normal University, Nanjing 210046, P. R. China

1. Introduction

The principle of self-mixing interference (SMI) is a new measuring technique which is applied in interferometry since 1980's. When a portion of light emitted from a laser source is reflected or scattered back into the laser cavity by an external target, the reflected light will mix with the light inside the cavity, causing a modulation of the laser output power. The self-mixing interference comes from the optical feedback effect. People always tried to eliminate the optical feedback effect previously. Gradually people began to make use of it actively to measure some physical quantities, thus self-mixing interference technology was brought forth. Compared with conventional interferometers, self-mixing interferometer (SMI) is characterized by its capability of high performance with inexpensive experimental setup and an extremely simple and the potential in direct industrial applications for vibration and displacement sensing. The SMI is well adapted for displacement measurement of these micro structure devices where cooperative target like triple mirror retro-reflector target necessitated in some interferometers is not available.

2. Experimental setup and results

The schematic diagram of the self-mixing interferometer with sinusoidal phase modulation is illustrated in Fig.1. A vertical polarized measurement light beam emitted by a He-Ne laser propagated through a various neutral density (ND) filter, an electro-optic modulator (EOM) and then reflected back to the laser cavity by a movable object, forming the self-mixing effect. Therefore, laser operations are altered and the self-mixing interference signal is monitored by a photodiode (PD) placed behind the back mirror of the laser. A sinusoidal phase modulation is obtained by varying of the optical length between the laser and object through an electro-optical crystal. The polarization of the light beam is set parallel to the electro-optically active axis of the EOM. The sinusoidal output of the signal generator is transferred to the EOM and pure sinusoidal modulation with extremely low insert-loss is generated. The object is fixed on a commercial PZT which can obtain displacement accuracy of 1 nm. When the signal processing unit sends a signal to the PZT controller, the object is moved a measured displacement ΔL. The output signal of PD is fed into the signal processing unit to retrieve the measured displacement in real time. To evaluate its performance, the sinusoidal phase modulating self-mixing interferometer was developed as shown in Fig.2. a commercial heterodyne interferometer (5529A, Agilent Co., USA) with 1 nm resolution was used to test the displacement of the same object for comparison. Fig. 3 show that the displacement reconstruction result of PZT with frequency 10HZ and amplitude from 200 nm to 1800 nm, the maximum error is 8nm. Fig. 4(a) show that Single displacement measurement results, the maximum error is 18nm. Fig.4(b) show that Times average displacement measurement results, the maximum error is 12 nm.

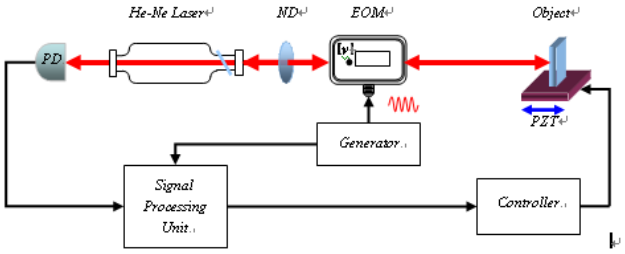

Fig.1. Schematic diagram of the self-mixing interferometer with phase modulation

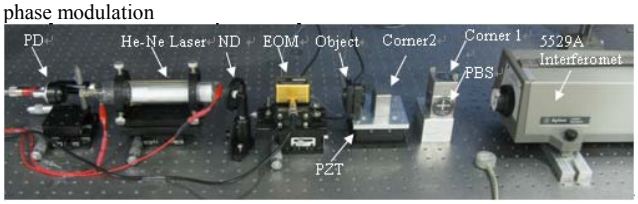

Fig.2. Photo of experimental setup.

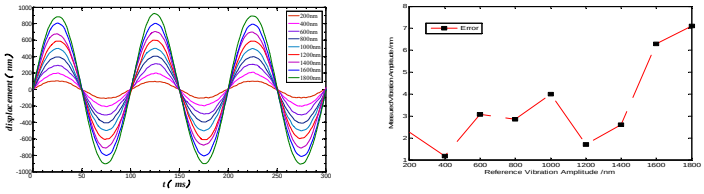

Fig.3. The displacement reconstruction result

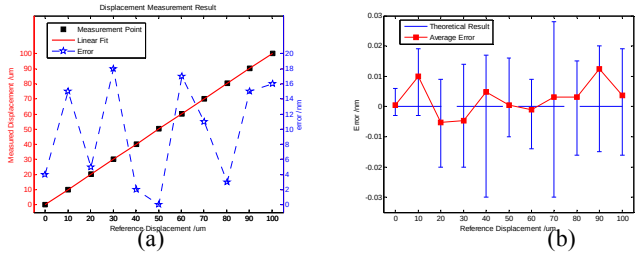

(a) (b)

Fig.4 Single displacement measurement results and times average displacement measurement results

Conclusion

The numerical simulation and experimental results show that the proposed new method can effectively demodulate the phase of the interference signal with high accuracy of less than 20 nm. Self-mixing interferometer (SMI) is characterized by its capability of high performance with an extremely simple and inexpensive experimental setup and the potential in direct industrial applications for vibration and displacement sensing .

References

[1] W. Ming, et al, Optics & Laser Techno. **33(6),** 409-416(2001).
[2] D. Guo, et al., Opt. Express, **13**, 1537-1543(2005).